AIAA JOURNAL
Vol. 59, No. 4, April 2021

Influence of the Ground, Ceiling, and Sidewall on Micro-Quadrotors

Darius J. Carter,* Lauren Bouchard,† and Daniel B. Quinn‡
University of Virginia, Charlottesville, Virginia 22903

https://doi.org/10.2514/1.J059787

The growth of the micro-aerial vehicle (MAV) industry is outpacing our understanding of how MAVs behave in cluttered environments. Search and rescue and product delivery (two key MAV applications) occur in tight, confined spaces filled with complex obstacles. Our current understanding of how micro-quadrotors interact with boundaries is based primarily on helicopter models, which were designed for high-Reynolds-number single-rotor flows. To test how well existing near-boundary models apply to micro-quadrotors, the thrust forces and wakes of a micro-quadrotor near a ground, ceiling, and sidewall were measured. It is found that micro-quadrotors (like their larger counterparts) experience a large boost in lift near the ground/ceiling and a slight drop in lift near the sidewall. Particle image velocimetry is used to quantify the velocity around the rotors and evaluate the assumptions made by existing ground and ceiling models. Complex boundary-layer interactions were observed at low altitudes, especially when the quadrotor was tilted relative to the ground. Reduced-order modeling was also used to explore the safety implications of near ground/ceiling flight. Tradeoffs between safety and efficiency that are sensitive to the ground/ceiling models were discovered, highlighting the need for precise near-boundary models. The results of this study therefore offer guidance for near-boundary model-driven controllers that could improve situational awareness and sensorless landings.

Nomenclature

C_L	=	rotor lift coefficient
C_P	=	rotor power coefficient
f	=	rotor frequency
g	=	acceleration due to gravity (9.8 $\mathrm{m/s^2}$ in this study)
I	=	vehicle rolling moment of inertia (2–3 $\times 10^{-5}$ $\mathrm{kg \cdot m^3}$ in this study)
J	=	rotor advance ratio ($\dot{z}/[2rf]$)
L	=	lift
L_∞	=	lift far from the boundary
L'	=	simulated lift disturbance
ℓ	=	distance between centers of rotors (90 mm in this study)
$\hat{\ell}$	=	ℓ scaled by rotor radius ($\hat{\ell} \equiv \ell/r$; 3.9 in this study)
m	=	vehicle mass (27 g in this study)
r	=	rotor radius (23 mm in this study)
$\boldsymbol{u}$	=	in-plane flow velocity
$\boldsymbol{u}_\infty$	=	in-plane flow velocity far from boundaries
z	=	distance from rotor center to ceiling/ground/sidewall
z_0	=	target height (of the rotor)
$\hat{z}$	=	z scaled by rotor radius ($\hat{z} \equiv z/r$)
$\hat{z}_0$	=	z_0 scaled by rotor radius ($\hat{z}_0 \equiv z_0/r$)
ΔL	=	relative change in lift near a boundary, $(L - L_\infty)/L_\infty$
θ_{tilt}	=	horizontal tilt angle between quadrotor and boundary
ρ	=	density of air (1.2 $\mathrm{kg/m^3}$ in this study)

I. Introduction

MICRO-AERIAL vehicles (MAVs) are growing in popularity due to their low cost and high agility. Quadrotors are especially useful because of their ability to hover and perform precise movements. Their small size lets quadrotors navigate in narrow corridors such as those of urbanscapes and collapsed mines, places that are inaccessible to conventional vehicles. However, these new environments lead to new challenges. Micro-quadrotors are inherently unstable due to their small size and low speeds [1–3], and they can be further destabilized by their close proximity to boundaries like walls, grounds, and ceilings [4].

One solution for handling near-boundary effects is to use data-driven control. Reinforcement learning [4] and adaptive control [5], for example, have been used to train quadrotors to fly near boundaries, and centralized predictive interaction control has helped protect quadrotors from crashing into the ceiling [6]. However, even in simple environments, model uncertainty can cause data-driven quadrotor controllers to fail [7]. Aerodynamic models are therefore incorporated into many controllers to improve performance. Some state estimators have used blade element theory [8] or wind models [9] to improve stability. In other cases, aerodynamic models have enabled control compensation in near-boundary maneuvers and landings [10–13].

When high-precision control is not necessary, data-driven reactive approaches may be sufficient. However, many high-impact quadrotor applications, package delivery in crowded buildings, search-and-rescue in rubble corridors, coordinated swarming, etc., require centimeter-scale precision. Data-driven control is especially problematic if sensors are compromised by sand/dust or low lighting, because the limited payload capacity of quadrotors may preclude redundancy in their sensing systems [14]. Another key advantage of using model-based control is its importance to the future of MAV regulation. As MAVs become more mainstream, their regulation will demand physics-based models that can guarantee provably safe operation.

A challenge of model-based quadrotor control near boundaries is that existing models are rooted in helicopter theories. These classic theories use the method of images to model a helicopter's lift near the ground [15]. However, quadrotors have three additional rotors, and their smaller Reynolds numbers lead to viscous effects that are negligible at helicopter scales [16]. Recently, classic theories have been adapted with an empirical coefficient that accounts for the extra rotors [17]. Ceiling and sidewall effects have no history in helicopter research, so they are relatively unexplored in comparison. The first attempt at a near-ceiling model was made by Hsiao and Chirarattananon [18], who used blade element momentum theory to predict the increased lift seen near the ceiling. New models have inspired recent analytical and experimental studies that clearly demonstrate the advantages of near-ceiling flight, which are particularly relevant for bridge-inspection MAVs [19–21]. How well these near-boundary models apply to micro-quadrotors (rotor radius $r < 50$ mm) is unknown.

To contribute to the growing field of near-boundary quadrotor research, we investigated the forces on a micro-quadrotor (Crazyflie

Received 13 May 2020; revision received 18 September 2020; accepted for publication 14 November 2020; published online 15 December 2020.

*Graduate Student, Mechanical and Aerospace Engineering. Student Member AIAA.
†Graduate Student, Mechanical and Aerospace Engineering.
‡Assistant Professor, Mechanical and Aerospace Engineering, and Electrical and Computer Engineering.

2.0) near the ground, ceiling, and sidewall. Like groups that considered larger quadrotors [17,22], we found power law dependencies between lift and ground proximity. In some regimes, however, existing models underpredicted the ground's effect and overpredicted the ceiling's effect. We therefore used particle image velocimetry (PIV) to explore the time-averaged flowfields surrounding the micro-quadrotors. We found that standing vortices beneath the quadrotor were highly sensitive to quadrotor attitude, and we did not observe the fountain effect seen beneath larger quadrotors [17]. These effects may account for some of the differences experienced by micro-quadrotors. To explore how our analyses scale, we ran reduced-order simulations of quadrotors hovering near the ground and ceiling. Based on the results, we show how improved near-boundary models could help to quantify tradeoffs between efficiency and safety.

II. Experimental Methods

To investigate how boundaries affect micro-quadrotors, we built a glass and high-density polyethylene (HDPE) flight arena (1.5 m × 1.5 m × 1.5 m) (Fig. 1). For our first round of tests, we mounted a micro-quadrotor (Crazyflie 2.0, rotor radius $r = 23$ mm) to a 1 kg load cell (Omega LCFD, ±1.5 g accuracy) in the center of the arena. The load cell was suspended from a custom traverse that positioned the quadrotor near a horizontal plane or a sidewall. We chose the Crazyflie because of its open-source support and its popularity in the hobbyist community, and we chose a tethered arrangement so we could measure time-averaged flowfields and collect force data simultaneously. Boundary proximity z is the distance between the rotor midline and the ground/ceiling/sidewall (in the sidewall cases, proximity is measured from the rotor nearest to the wall). Ceiling tests were done by inverting the quadrotor and using the same horizontal plane. We checked that orientation had negligible effects by comparing flowfields between upright and upside-down cases (along typical streamlines in our setup, dynamic pressures are about 50 times higher than gravitational pressures).

At 20 different distances from the ground/ceiling/sidewall (see Table 1), we recorded time-averaged lift for 4 throttle levels: 25, 50, 75, and 92% (max reliable throttle). For reference, Crazyflies with no payload hover at 60% throttle. The traverse automatically visited each distance 15 times in a randomized order, averaging 10 s of lift at 1000 Hz for each trial. The force sensor was re-zeroed between each trial to minimize sensor drift between trials, and no observable drift took place within each trial. To facilitate comparisons between cases, we calculated the percent increase of net lift compared with its value far from boundaries: $\Delta L \equiv (L - L_\infty)/L_\infty$.

To measure the flow around the Crazyflie, we used PIV to track neutrally buoyant particles in the arena. The PIV system used a dual-cavity pulse laser (Litron, 200 mJ @ 15Hz) to illuminate aerosolized particles of glycol and water (diameter 14 μm) in a plane through the center of two of the rotors. Particle motion was triangulated by two high-speed cameras (Phantom SpeedSense M341, 4MP) that fed into cross-correlation software (Dantec Dynamic Studio). Based on a convergence test, we determined that 150 image pairs (10 s of data) were sufficient for time-averaged velocity fields to converge to <0.1%

Table 1 Distances from the boundary during tethered experiments

Distance to ceiling (cm)	Distance to ground (cm)	Distance to sidewall (cm)
5	57	15
6	58	16
7	59	17
8	60	18
9	61	19
10	62	21
11	63	22
12	64	23
14	66	24
15	68	26
18	70	28
22	74	32
25	77	35
29	82	40
34	86	44
38	90	48
55	108	66
68	121	79
90	142	101
525	577	535

of the average projection error per 10 μm. The result of the averaged cross-correlations is a grid of velocity vectors, one for each 32 px × 32 px window.

We used the velocity grids to plot airspeed density and trace streamlines (DensityPlot and StreamPlot in Mathematica 10). Areas that were unobservable due to poor contrast near the illuminated Crazyflie are shown as grayed areas in the figures. A light reflection caused the one-pixel outlier seen in the ceiling case. Downwash velocities were estimated by using a cross section of the wake 1 rotor diameter beneath each rotor. The momentum jet was angled slightly to the left in some flowfields near the ground (see Results and Fig. 4), which motivated us to test the sensitivity to rotor angle. We therefore ran an additional set of tests with the artificial ground plane at six angles off the horizontal (+4.6°, +3.1°, +1.5°, −1.7°, −3.2°, −4.9°; each ±0.05°).

III. Mathematical Models

The first attempt to model rotors in ground effect was done for helicopter landings. Cheeseman and Bennett [15] used mirrored source elements (method of images) to model the lift of a rotor (L) as it approaches the ground. Hayden [23] later added power to the model using a correlation based on flight test data. In the model, the rotor's image leads to downwash velocities at the rotor plane. The result is an increase in rotor lift compared with its value far from the ground (L_∞). Near-ground lift therefore depends on the altitude z according to

$$\frac{L}{L_\infty} = \frac{1}{1 - (1/16\hat{z}^2)} \tag{1}$$

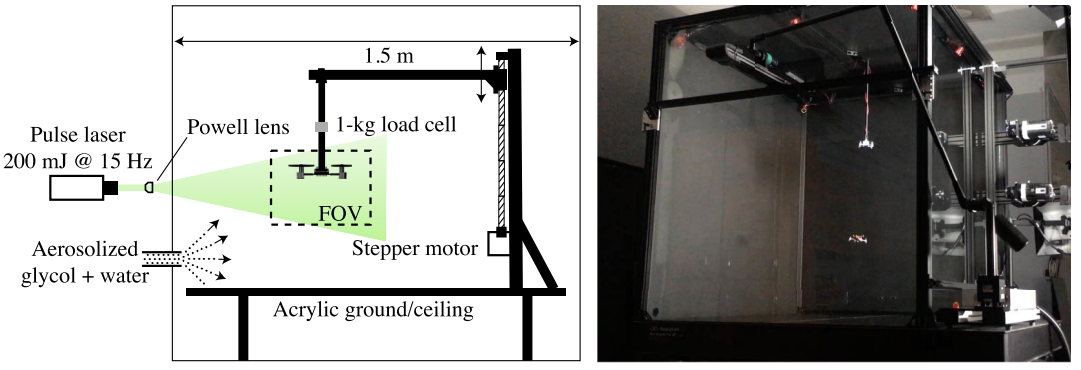

Fig. 1 A glass arena was used to measure the lift of a tethered Crazyflie and the surrounding flowfield via particle image velocimetry.

where $\hat{z}$ is the altitude scaled by rotor radius ($\hat{z} \equiv z/r$). The method, which is based on potential flow theory, assumes that the flow is incompressible and inviscid. It also assumes that the downwash is constant across the rotor disk, that the rotor disk is infinitely thin, and that $\hat{z} > 0.25$.

To account for the extra rotors of a quadrotor, Sanchez-Cuevas et al. [17] modeled four sources (arranged in a square with side length ℓ) and then applied the method of images. A secondary effect of there being four rotors comes from the quadrotor's symmetry. The flows from the four jets converge beneath the quadrotor, rise up in the center, further reduce the downwash at the rotor planes, and therefore cause an increase in lift. To account for this fountain effect [17], Sanchez-Cuevas et al. added a semi-empirical term with a fitted coefficient K_b. Their modified expression for near-ground lift is

$$\frac{L}{L_\infty} = \frac{1}{1 - \frac{1}{16\hat{z}^2} - \frac{\hat{z}}{\sqrt{(\hat{\ell}^2+4\hat{z}^2)^3}} - \frac{\hat{z}}{2\sqrt{(2\hat{\ell}^2+4\hat{z}^2)^3}} - \frac{\hat{z}}{2K_b\sqrt{(\hat{\ell}^2+4\hat{z}^2)^3}}} \tag{2}$$

where $\hat{\ell} \equiv \ell/r$. The model is based on the same assumptions as the original helicopter theory [15]. Sanchez-Cuevas et al. found good agreement with experimentally calculated lift when $K_b \approx 2$.

Ceiling effect analysis is fairly new because previous ground effect studies were done for helicopter flight. Hsiao and Chirarattananon [18] modeled ceiling effect using blade element momentum theory and a control volume analysis. They found that, like in ground effect, the presence of the boundary decreases the downwash velocity at the rotor plane. Their model predicts a sharp increase in rotor lift near the ceiling, an effect that has been confirmed in experiments [6]. Specifically, their model predicts that

$$\frac{L}{L_\infty} = \frac{1}{2} + \frac{1}{2}\sqrt{1 + \frac{1}{8\hat{z}^2}} \tag{3}$$

where here z is the distance between the rotors and the ceiling plane. Like ground effect theories, the model assumes that the flow is incompressible and inviscid, that the rotor disk is infinitely thin, and that the downwash through the rotor is uniform. They further assumed that the flow entering a control volume above the rotors was entirely horizontal. All of these models assume hovering flight, i.e., an advance ratio ($J \equiv \dot{z}/(2rf)$) of zero, and assume lift coefficients that are independent of Reynolds number and rotor solidity.

IV. Numerical Methods

To investigate the implications of boundary effects on MAV safety, we created a reduced-order simulation capturing the vertical dynamics of near-boundary quadrotors to determine relative crash propensities. The simulation allowed us to compare crash rates of different boundary models across a range of flight altitudes, using the Crazyflie's dimensions ($r = 23$ mm, $\ell = 90$ mm) and weight (27 g) as an example. We also analytically estimated the relative power required to maintain a given altitude. This information, together with the crash propensities, highlights efficiency-safety tradeoffs inherent in near-boundary flight.

The reduced-order model considers three forces acting on the Crazyflie: the lift force (L), the vehicle's own weight (mg), and random vertical forces chosen to simulate disturbances (L'). These random forces were generated by a white Gaussian noise function (mean of 0 N and standard deviation of 0.015 N). From a force balance, the vehicle's acceleration follows as

$$\ddot{z}(t) = \frac{L(z(t)) + L'(t) - mg}{m} \tag{4}$$

that we solved using a Euler integration (time step of 0.1 s) to determine velocity and position over 120 s. At every time step, L was recalculated as a function of the vehicle's current altitude z and the rotor frequency f (the control variable).

To estimate L at distances far from a boundary, the simulations used blade element theory: $L = 4C_L\rho f^2 r^4$, where C_L is the lift coefficient of the rotor blade. We included the 4 to account for the four rotors, and we held C_L constant at 1.6 (in doing so, we assumed lift coefficient to be independent of Reynolds Number). This lift force served as L_∞ for the calculation of the near-boundary lift indicated by the Hsiao–Chirarattananon and Sanchez-Cuevas models [Eqs. (2) and (3)]. We used Sanchez-Cuevas's empirically fit $K_b = 2$ in our ground effect model [17]. To avoid unreasonably large lift values (and the singularity near $\hat{z} = 0.25$ in the ground model), we bounded L/L_∞ to its value computed at $\hat{z} = 0.5$. To assess the sensitivity of vehicle safety to the accuracy of the boundary model, we also simulated vehicle dynamics with boundary models scaled by powers of 0.6, 0.8, 1.2, and 1.4. For example, the lift in one simulation would be computed as $(L/L_\infty)^{1.4}$, such that the lift is always greater than L/L_∞ indicated by the model yet still approaches L_∞ at distances far from the boundary.

We commanded the vehicle to maintain a target height (measured as distance from the rotor to the boundary) throughout each simulation using a simple proportional-integral-derivative (PID) controller on the rotor frequency. At each time step, the frequency was determined by

$$f = k_P(z - z_0) + k_D\dot{z} + k_I\int_0^t (z - z_0)\,\mathrm{d}t + f_0 \tag{5}$$

where z_0 is the target height, f_0 is a frequency offset, and k_P, k_D, and k_I are the controller gains. Gains were held constant across all simulations. The k_P and k_D gains were chosen such that a quadrotor hypothetically launched from the ground would quickly reach its desired altitude with minimal overshoot; we decided upon $k_P = 316\ \mathrm{m^{-1}} \cdot \mathrm{s^{-1}}$ and $k_D = 316\ \mathrm{m^{-1}}$. Because we ultimately wanted the vehicle to start at and maintain a given height throughout our simulations, we added a frequency offset sufficient to counter the Crazyflie's own weight (adjusted for increased lift due to the boundary effect in applicable simulations). Although an integral gain was still necessary to account for any asymmetry in the disturbances, including this offset meant that a relatively small integral gain of $31.6\ \mathrm{m^{-1}} \cdot \mathrm{s^{-2}}$ was sufficient to consistently maintain a desired average altitude. The minimum rotor frequency was also bounded at 0; i.e., the rotors could not spin backward to provide downward thrust in the event that the altitude far exceeded the target height.

Vehicle target heights ranged from $\hat{z}_0 \approx 0.5$ to 2 above ground and $\hat{z}_0 \approx 1$ to 2.5 below the ceiling (where $\hat{z}_0 \equiv z_0/r$). If at any time during the simulation $\hat{z} \leq 0$, we considered the vehicle to have crashed into the boundary and thus stopped the simulation, adding to a counter whenever this happened. Simulations of each combination of setpoint and boundary model magnitude were repeated 1000 times to determine an average crash rate at each parameter combination.

In contrast, the relative energy cost of hovering near a boundary can be determined analytically because it reduces to a function of our boundary model. We combined our lift models with blade element theory, which provides the mechanical power generated by a rotor as $C_P\rho f^3 r^5$, where C_P is the power coefficient. For the small advance ratios ($J \equiv \dot{z}/(2rf)$) of hovering, C_L and C_P are relatively constant (e.g., <5% change for $J < 0.2$ for a typical rotor [24]). The ratio of power consumed in two different flight conditions 1 and 2 is therefore $\approx(f_1/f_2)^3$. Inverting $L = C_L\rho f^2 r^4$ gives the frequency f required for hover as a function of $\sqrt{L}$. Therefore, the mechanical power generated near a boundary compared with the power far from the boundary ("relative energy cost") is $(L/L_\infty)^{-3/2}$, where L/L_∞ follows from Eqs. (2) and (3).

V. Results

A. Tethered Force Measurements

Our tethered force measurements confirm that micro-quadrotors, like their larger counterparts [17], see a boost in lift near the ground (Fig. 2a). The lift increase that we measured (up to 20%) was more than twice what classic theory predicts [15]. Sanchez-Cuevas et al. [17] observed similarly high lift values and attributed the deviation from theory to the fountain effect. When we use their one-parameter fit for modeling fountain effect [Eq. (2)], we see a good match ($R^2 = 0.956$) for $1 < \hat{z} < 3$. This suggests that their semi-empirical model scales well to smaller quadrotors. Figure 2 includes all four of the throttles we

considered; the collapse to a single curve illustrates that the relative lift increase near boundaries is insensitive to air flow speeds. For comparison, we show existing quadrotor data, classic helicopter theory [C-B Model; Eq. (1)], and the Sanchez-Cuevas model [S-C model; Eq. (2)] with its original fit (PQuad; $r = 120$ mm, $K_b = 2$) and a new fit (Crazyflie; $r = 23$ mm, $K_b = 2$).

Near the ceiling, the Crazyflie experienced a sharp increase in lift (up to 60%) very close to the boundary (Fig. 2b). Our data go to lower $\hat{z}$ values near the ceiling because the underside of the quadrotor prevents closer ground proximities. Like larger quadrotors, the Crazyflie had to be closer to the ceiling than the ground to experience the same increase in lift [17,22]. Near the ground, effects on rotor lift were significant when $\hat{z} < 4$; near the ceiling, effects were significant only when $\hat{z} < 1$. The ceiling model of Hsiao and Chirarattananon [18] gives a good estimate of the lift increase except for very low $\hat{z}$ values, where the model overpredicts our measurements.

Unlike near the ground and ceiling, the lift decreases slightly (<5%) near a sidewall (Fig. 2c). The sidewall effects are small in comparison to those seen near the ground and ceiling. The quadrotor has to be very close to the wall before changes in lift are noticeable ($|\Delta L| > 2\%$ for $\hat{z} < 0.3$). This proximity, corresponding to just a few millimeters, would be outside the scope of most applications. However, unlike the ceiling and ground, which has a symmetric effect on the rotors, the sidewall presumably affects the rotors unequally, which would lead to destabilizing rolling torques. These torques are known to affect larger quadrotors [5]. For the Crazyflie, it appears that differential lifts of up to $\approx 0.03 L_\infty$ are possible very close to the wall (Fig. 2c). Using the mass and moment of inertia of the Crazyflie (27 g, $2\text{–}3 \times 10^{-5}$ kg · m^2 [25]), we estimate rolling torques of ≈0.2 N mm and angular accelerations of ≈400 deg/s^2.

B. Flowfield Measurements

Motivated by the slight differences between our measurements, existing models, and existing data for larger quadrotors, we conducted PIV to measure the time-averaged flowfields around the Crazyflie (Fig. 3). To avoid a laser shadow, we measured the flow around one rotor and reflected across the midplane the Crazyflie. The wake of the rotors is significantly different near boundaries, particularly near the ground. The ground causes each rotor wake to diverge into two momentum jets. Near both the ground and the ceiling, PIV reveals a reduction in the rotor downwash of ≈22% (ceiling) and 6% (ground). In comparison, the classic model of Cheeseman and Bennett predicts only a 0.4% decrease in downwash at the same ground proximity. This discrepancy helps to explain why our lift increase near the ground was higher than what classic theory predicts (Fig. 2a).

To better understand how the ground affected the flow, we considered multiple ground proximities and compared with the control case (Fig. 4). In the comparison, negative values imply that the flow is slower than the control case; positive values imply that the flow is faster. As the Crazyflie approaches the ground, the momentum of the rotor wake is directed to either side, leaving a triangular stagnation zone beneath the rotor. As $\hat{z}$ decreases further, the stagnation zone grows until it nearly reaches the bottom of the quadrotor. Quasi-steady analyses would suggest high pressures in this zone, which could help to explain why the ground causes lift to increase even at relatively high $\hat{z}$ values (up to ≈4). Compared with the control case, the near ground wakes also show relatively high airspeeds just outside the stagnation zone. These higher airspeeds are particularly pronounced very close to the wall (Fig. 4, $\hat{z} = 2.6$, $\hat{z} = 1.8$), suggesting that near-ground dynamics may also be affecting jet entrainment below the rotor.

In comparison to the ground, the change in downwash of the ceiling on the flow was less pronounced (Fig. 4). For the first two cases we

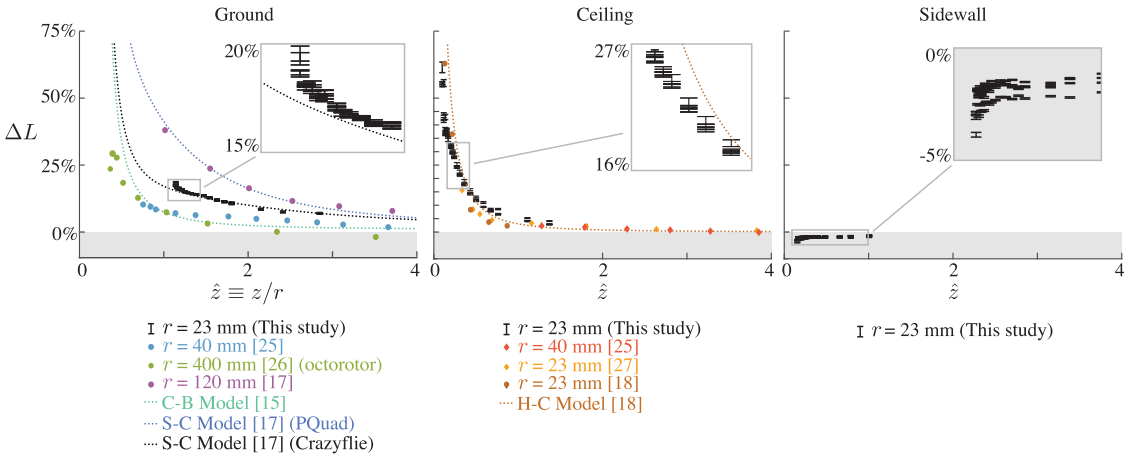

Fig. 2 A comparison of recent modeled and experimental data for quadrotors near the sidewall, ceiling, and ground.

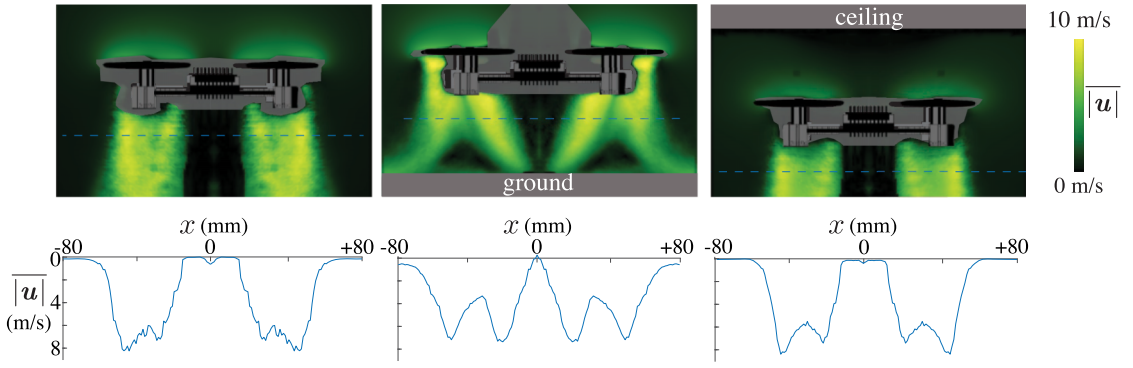

Fig. 3 Time-averaged velocities near the ground ($\hat{z} = 3.4$, center) and ceiling ($\hat{z} = 2$, right) differ in direction and strength compared with the control ($\hat{z} \gg 1$, left). Velocity cross sections shown below.

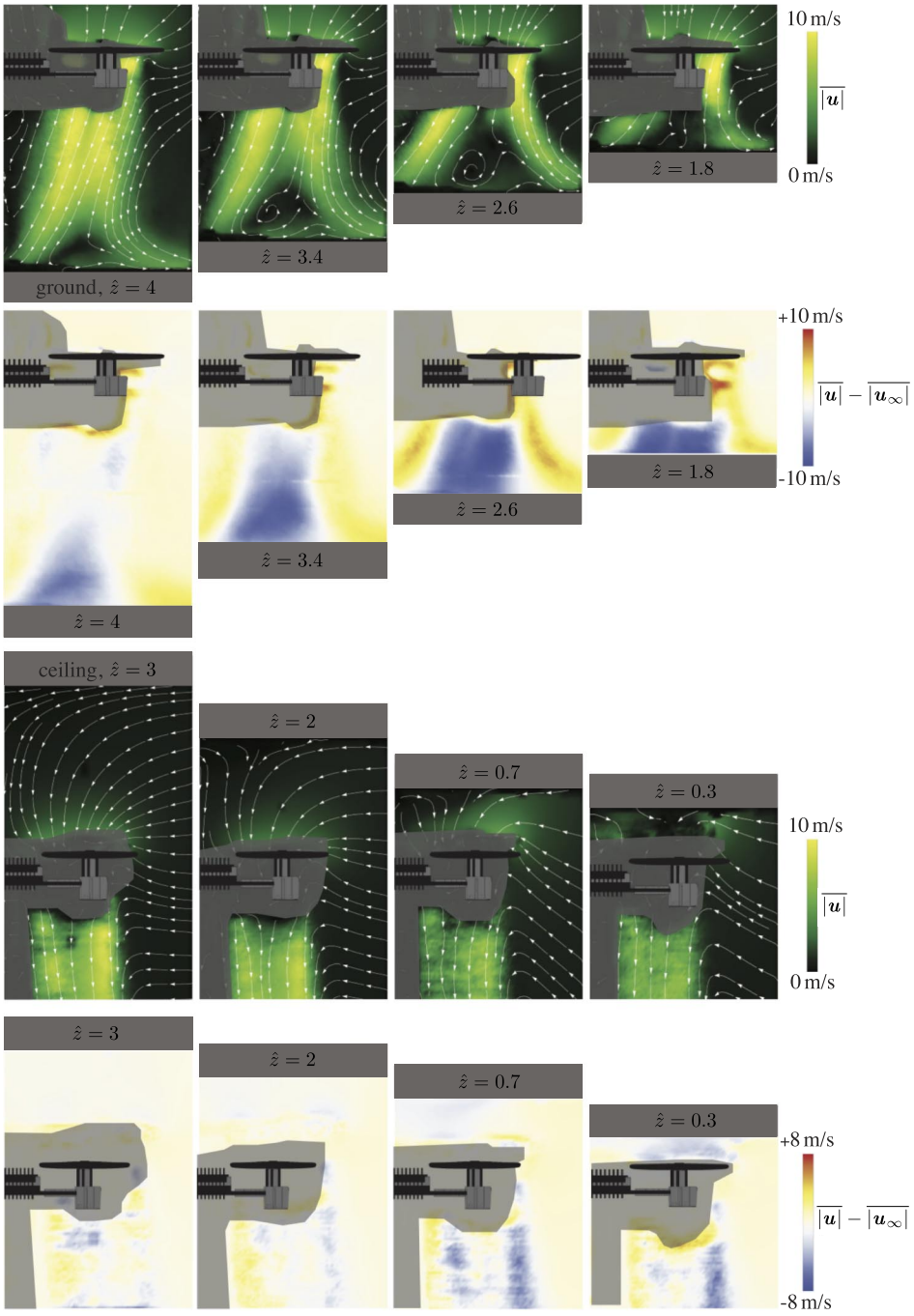

Fig. 4 Time-averaged velocities near the ceiling/ground are compared against the control to highlight areas of high variation.

considered ($\hat{z} = 3$, $\hat{z} = 2$), the flowfields are almost identical to the control case. In contrast, even when $\hat{z} = 4$ near the ground, the flow is significantly altered by the boundary (Fig. 4). This difference is consistent with our lift results (Figs. 2a and 2b), which showed how lift was affected at higher $\hat{z}$ values near the ground compared with the ceiling. As $\hat{z}$ reduces further near the ceiling ($\hat{z} = 0.7$ and $\hat{z} = 0.3$), the flow both above and below the rotor becomes less uniform than in the control case. The streamlines bringing air to the rotors now approach at an upward angle, and the airspeeds are slower just above the rotor and beneath the rotor tips.

To test the sensitivity of rotor angle, we also performed PIV with rotated ground planes (Fig. 5). We observed no noticeable effects of rotor tilt angle on the flow above the rotor. In contrast, the wake beneath the rotor was considerably affected by tilt angle. In all cases, the jet beneath the rotor split in two and left a region of slow-moving flow, as we had seen previously. However, the topology of the split and the streamlines in the slow-moving region were very sensitive to tilt angle. At some tilt angles ($\theta_{\text{tilt}} = +4.6°, +3.1°$), two stable pairs of counter-rotating vortices are seen beneath the rotor. As the tilt angle decreases, the vortices are replaced by a single counterclockwise vortex. This sensitivity could explain some of the asymmetries seen in the jet near the ground. Even slight imperfections in rotor tilt angle could cause different wake dynamics in and around the stagnation zones beneath the rotors.

C. Near-Boundary Simulations

Our reduced-order simulations demonstrate that the ground has a stabilizing effect while the ceiling has a destabilizing effect. Random fluctuations cause the quadrotor to deviate from its target height, which could potentially lead to crashes with a nearby boundary. However, as a quadrotor approaches the ground, the heightened lift pushes the quadrotor upward and prevents a crash (Fig. 6a). In contrast, approaching a ceiling leads to higher forces toward the boundary, which can

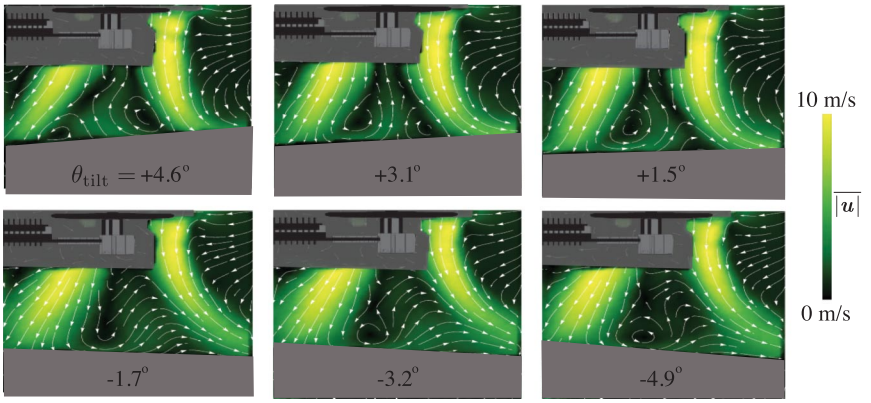

Fig. 5 Time-averaged velocities near a horizontally tilted ground plane show the sensitivity of the Crazyflie's wake to tilt angle.

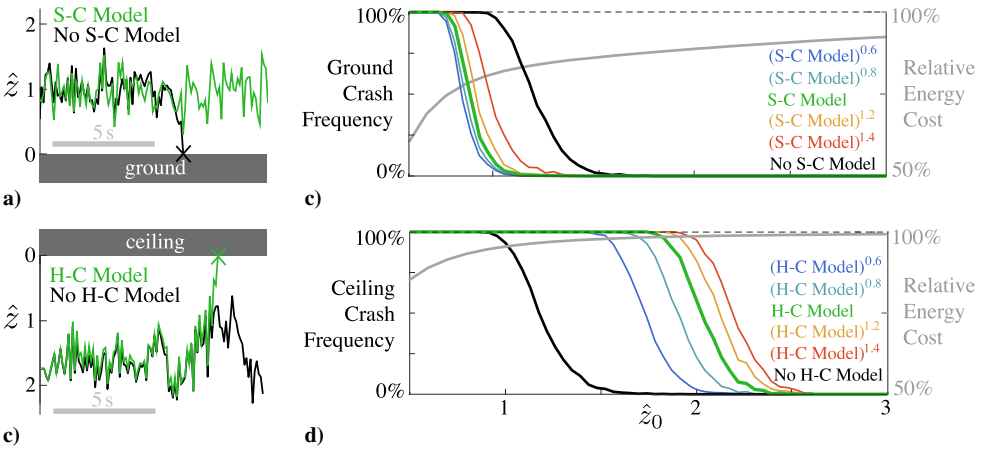

Fig. 6 Reduced-order quadrotor simulation. a,b) Sample time histories with and without the ground/ceiling models. c,d) Average crash frequencies with and without ground/ceiling models (scaled by exponentiation).

result in a crash (Fig. 6b). To explore the likelihood of crashes, we aggregated hundreds of trials and looked at average crash rates.

On average, the simulated quadrotor crashes less near the ground when a ground model is included in the simulation. With no boundary model, random fluctuations cause crashes as high as $\hat{z}_0 \approx 1.5$ (Fig. 6c). When a ground model is added, the quadrotor can be about half of a rotor radius closer to the ground before this rise in crash rate. Scaling the ground model causes only slight changes in the $\hat{z}_0$ value at which this rise occurs.

Unlike a quadrotor near the ground, a quadrotor near the ceiling experiences more crashes. On average, the quadrotor is likely to crash into the ceiling when $\hat{z}_0 < \approx 2$ (Fig. 6d). Scaling the models has a stronger effect on the safe $\hat{z}_0$ range near the ceiling than it does for the safe range near the ground. The effects differ in magnitude because they are caused by different mechanisms. The ground acts as a buffer that pushes the quadrotor away; crashes require large random fluctuations. The ceiling acts as an attractor, pulling the quadrotor into a positive lift feedback loop; crashes are inevitable unless the controller can reverse course in time.

For comparison, we also plotted the relative energy costs of near-boundary flight in order to highlight the tradeoff between safety and efficiency. This relation makes it clear why near-boundary flight is more efficient: as $\hat{z}$ drops, L/L_∞ goes up, requiring a smaller rotor frequency and less energy to maintain altitude. Chances of crashing increase with smaller $\hat{z}_0$, however, so accurate models are critical for balancing safety and efficiency near the ground/ceiling (Figs. 6c and 6d).

Note that the value of the safe/unsafe $\hat{z}$ values depends on the disturbance intensity and the PID gains injected into our model. Varying the intensity or the gains would rescale the $\hat{z}$ values in Fig. 6, though the relative positioning of the curves, and therefore our conclusions about crash frequency, would be unaffected. If the equation of motion [Eq. (4)] were nondimensionalized, say, by using rotor radius and gravity to scale lengths and times ($\hat{z} \equiv z/r$, $\hat{t} \equiv t/\sqrt{r/g}$), it could be written as

$$\ddot{\hat{z}} = \left(\alpha(\hat{z} - \hat{z}_0) + \beta\dot{\hat{z}} + \gamma\int_0^{\hat{t}}(\hat{z} - \hat{z}_0)\,\mathrm{d}\hat{t} + \delta\right)^2 + \frac{L'}{mg} - 1 \qquad (6)$$

where the four dimensionless groups α, β, γ, and δ are the controller gains and offset scaled by physical variables: $k_\mathrm{P}\sqrt{4C_\mathrm{L}\rho r^6/(mg)}$, $k_\mathrm{D}\sqrt{4C_\mathrm{L}\rho r^5/m}$, $k_\mathrm{I}\sqrt{4C_\mathrm{L}\rho r^7/(mg^2)}$, and $f_0\sqrt{4C_\mathrm{L}\rho r^4/(mg)}$, respectively. If lift coefficient were not assumed to be independent of the blade-tip Reynolds number (see Numerical Methods section), Reynolds number would be an additional dimensionless group that includes viscosity ($\rho f r/\mu$, where μ is viscosity). Therefore, although our simulations were run with variables specific to a Crazyflie, they could be tested for quadrotors more generally by tuning $\alpha, \beta, \gamma, \delta$, and the disturbance function scaled by vehicle weight (L'/mg).

VI. Conclusions

In general, the Sanchez-Cuevas model works well to model the lift forces we observed near the ground. The same K_b value that they used to account for the fountain effect (2) also fit our data well (Fig. 2). In the final few altitudes we tested, just before the quadrotor touched the ground, our lift results began to deviate from the Sanchez-Cuevas model. We did not see strong evidence of an upward jet beneath the rotors (Figs. 3 and 4), which could perhaps explain the discrepancy. However, there may be an upward jet beneath the center of the quadrotor, out of the plane of the laser. Understanding these subtle changes in the rotor wakes is important for developing more advanced near-boundary models, especially because rotor–rotor interactions also affect performance [26].

In light of our tilt analysis (Fig. 5), modeling secondary vortices may also help improve near-ground MAV models. The robust appearance of the vortices in time-averaged flowfields suggests that they are stable. However, their topology is sensitive to tilt angle, and they can disappear with even slight ($\approx 3^\circ$) changes in attitude (Fig. 5). We did not record any significant sensitivity to tilt angle in the thrust, so these vortices may play a minor role in scaling the time-averaged forces/torques on the vehicle, but their appearance could have important implications for landing stability or ground particle dispersion.

Except for very close ceiling proximities, the ceiling model from Hsiao and Chirarattananon [18] also gives good estimates of our lift results. It appears that both the Sanchez-Cuevas model and Hsiao and Chirarattananon model can scale down to micro-quadrotors. As for the deviation from model predictions that we see very close to the ceiling (Fig. 2, $\hat{z} < 0.5$), we suspect that viscous effects are no longer negligible over such small length scales. In the inviscid model of Hsiao and Chirarattananon, rotor downwash is assumed constant, the streamlines entering the control volume above the rotor are horizontal. Our PIV measurements reveal that these assumptions begin to break down very close to the ceiling. However, we expect that the more dominant effect is a change in pressure above the quadrotor caused by interactions between the rotor and the boundary layer on the ceiling.

One application of near-boundary models is sensorless boundary detection. Using known lift-altitude relations, a quadrotor could predict its proximity to a boundary based on throttle alone. This type of heightened situational awareness would be particularly helpful in situations where other sensing modalities may be compromised. Using a ground model has, for example, been shown to facilitate sensorless landings [11–13] and swarm-based blind terrain mapping [10]. Our force measurements and simulations offer design suggestions for this technique. The collapse we observed with throttle (Fig. 2) implies that model-based boundary detection could work with the same calibration even with different payloads. Sensorless sidewall detection is unlikely to be accurate enough based on changes in lift (Fig. 2c). The safety tradeoffs we demonstrated (Fig. 6) show that ground detection would be safer than ceiling detection. Our analysis further suggests that crash likelihood is not only a function of target height and boundary effects but also a function of dimensionless parameter groups involving the noise and the controller gains [Eq. (6)]. This could help formalize future design via nondimensionalization. For example, for different payloads (varying m), controller gains could be adapted to maintain the same α, β, and γ.

Perhaps the most promising application of near-boundary models is safer, more efficient path planning, especially in boundary-rich environments. It has been shown that flying near boundaries can save energy [18,19], and thus path-planning algorithms can be made more efficient by incorporating near-boundary models [13]. As the quadrotor approaches the ceiling/ground, energy savings increase (Figs. 2a, 2b, 6b, and 6d), but so do the chances of crashing (Figs. 6b and 6d). Path-planning algorithms that incorporate both safety and efficiency could balance the kind of tradeoffs we observed in our reduced-order modeling (Fig. 6). In applications where some crashes may be tolerable, the efficiency of near-boundary flight may be worth the added risk. Alternatively, a physical barrier could prevent ceiling crashes while maintaining the advantages of near-boundary flight, as has been demoed in bridge inspection MAVs [19]. Because of the sensitivity of these tradeoffs to model scale (Fig. 6d), it is critical to have near-boundary models with centimeter-scale precision. Our work confirms the effectiveness of recent ground and ceiling models [17,18] for micro-quadrotors and offers new ideas for improving the models further using near-boundary viscous effects.

Acknowledgments

This paper is based on the work supported by the University of Virginia and the National Science Foundation Research Traineeship program under Grant No. 1829004. The authors would like to thank Megan Mazzantenta, Qiang Zhong, and Bruce Zhang for assistance with experimental design, as well as the members of the Smart Fluid Systems Lab at the University of Virginia for their advice and support throughout this project.

References

[1] Mohamed, A., Massey, K., Watkins, S., and Clothier, R., "The Attitude Control of Fixed-Wing MAVS in Turbulent Environments," *Progress in Aerospace Sciences*, Vol. 66, April 2014, pp. 37–48. https://doi.org/10.1016/j.paerosci.2013.12.003

[2] Spedding, G., and Lissaman, P., "Technical Aspects of Microscale Flight Systems," *Journal of Avian Biology*, Vol. 29, Dec. 1998, pp. 458–468. https://doi.org/10.2307/3677165

[3] Theys, B., Dimitriadis, G., Andrianne, T., Hendrick, P., and De Schutter, J., "Wind Tunnel Testing of a VTOL MAV Propeller in Tilted Operating Mode," *2014 International Conference on Unmanned Aircraft Systems (ICUAS)*, Inst. of Electrical and Electronics Engineers, New York, 2014, pp. 1064–1072. https://doi.org/10.1109/ICUAS.2014.6842358

[4] Waslander, S. L., Hoffmann, G. M., Jang, J. S., and Tomlin, C. J., "Multi-Agent Quadrotor Testbed Control Design: Integral Sliding Mode vs. Reinforcement Learning," *2005 IEEE/RSJ International Conference on Intelligent Robots and Systems*, Inst. of Electrical and Electronics Engineers, New York, 2005, pp. 3712–3717. https://doi.org/10.1109/IROS.2005.1545025

[5] Lee, D., Awan, A., Kim, S., and Kim, H. J., "Adaptive Control for a VTOL UAV Operating near a Wall," *AIAA Guidance, Navigation, and Control Conference*, AIAA Paper 2012-4835, 2012. https://doi.org/10.2514/6.2012-4835

[6] Kocer, B. B., Tjahjowidodo, T., and Seet, G. G. L., "Centralized Predictive Ceiling Interaction Control of Quadrotor VTOL UAV," *Aerospace Science and Technology*, Vol. 76, May 2018, pp. 455–465. https://doi.org/10.1016/j.ast.2018.02.020

[7] Emran, B. J., and Najjaran, H., "A Review of Quadrotor: An Underactuated Mechanical System," *Annual Reviews in Control*, Vol. 46, Jan. 2018, pp. 165–180. https://doi.org/10.1016/j.arcontrol.2018.10.009

[8] Bristeau, P.-J., Martin, P., Salaün, E., and Petit, N., "The Role of Propeller Aerodynamics in the Model of a Quadrotor UAV," *2009 European Control Conference (ECC)*, Inst. of Electrical and Electronics Engineers, New York, 2009, pp. 683–688. https://doi.org/10.23919/ECC.2009.7074482

[9] Waslander, S., and Wang, C., "Wind Disturbance Estimation and Rejection for Quadrotor Position Control," *AIAA Infotech@Aerospace Conference*, AIAA Paper 2009-1983, 2009. https://doi.org/10.2514/6.2009-1983

[10] Powers, C., Mellinger, D., Kushleyev, A., Kothmann, B., and Kumar, V., "Influence of Aerodynamics and Proximity Effects in Quadrotor Flight," *Experimental Robotics*, Springer, Switzerland, 2013, pp. 289–302.

[11] Nobahari, H., and Sharifi, A., "Continuous Ant Colony Filter Applied to Online Estimation and Compensation of Ground Effect in Automatic Landing of Quadrotor," *Engineering Applications of Artificial Intelligence*, Vol. 32, June 2014, pp. 100–111. https://doi.org/10.1016/j.engappai.2014.03.004

[12] Danjun, L., Yan, Z., Zongying, S., and Geng, L., "Autonomous Landing of Quadrotor Based on Ground Effect Modelling," *2015 34th Chinese Control Conference (CCC)*, Inst. of Electrical and Electronics Engineers, New York, 2015, pp. 5647–5652. https://doi.org/10.1109/ChiCC.2015.7260521

[13] Gao, S., Di Franco, C., Carter, D., Quinn, D., and Bezzo, N., "Exploiting Ground and Ceiling Effects on Autonomous UAV Motion Planning," *2019 International Conference on Unmanned Aircraft Systems (ICUAS)*, Inst. of Electrical and Electronics Engineers, New York, 2019, pp. 768–777. https://doi.org/10.1109/ICUAS.2019.8798091

[14] Pines, D. J., and Bohorquez, F., "Challenges Facing Future Micro-Air-Vehicle Development," *Journal of Aircraft*, Vol. 43, No. 2, 2006, pp. 290–305. https://doi.org/10.2514/1.4922

[15] Cheeseman, I., and Bennett, W., "The Effect of the Ground on a Helicopter Rotor," Aeronautical Research Council R&M 3021, 1957.

[16] Ning, Z., Wlezien, R. W., and Hu, H., "An Experimental Study on Small UAV Propellers with Serrated Trailing Edges," *47th AIAA Fluid Dynamics Conference*, AIAA Paper 2017-3813, 2017. https://doi.org/10.2514/6.2017-3813

[17] Sanchez-Cuevas, P., Heredia, G., and Ollero, A., "Characterization of the Aerodynamic Ground Effect and Its Influence in Multirotor Control," *International Journal of Aerospace Engineering*, Vol. 2017, Jan. 2017. https://doi.org/10.1155/2017/1823056

[18] Hsiao, Y. H., and Chirarattananon, P., "Ceiling Effects for Hybrid Aerial-Surface Locomotion of Small Rotorcraft," arXiv preprint

arXiv:1905.04632, 2019.
https://doi.org/10.1109/TMECH.2019.2929589

[19] Sanchez-Cuevas, P., Heredia, G., and Ollero, A., "Multirotor UAS for Bridge Inspection by Contact Using the Ceiling Effect," *2017 International Conference on Unmanned Aircraft Systems (ICUAS)*, Inst. of Electrical and Electronics Engineers, New York, 2017, pp. 767–774.
https://doi.org/10.1109/ICUAS.2017.7991412

[20] Bahadir Kocer, B., Efe Tiryaki, M., Pratama, M., Tjahjowidodo, T., and Seet, G. G. L., "Aerial Robot Control in Close Proximity to Ceiling: A Force Estimation-Based Nonlinear MPC," arXiv, 2019, pp. arXiv–1907.

[21] Jimenez-Cano, A. E., Sanchez-Cuevas, P. J., Grau, P., Ollero, A., and Heredia, G., "Contact-Based Bridge Inspection Multirotors: Design, Modeling, and Control Considering the Ceiling Effect," *IEEE Robotics and Automation Letters*, Vol. 4, No. 4, 2019, pp. 3561–3568.
https://doi.org/10.1109/LRA.2019.2928206

[22] Hsiao, Y. H., and Chirarattananon, P., "Ceiling Effects for Surface Locomotion of Small Rotorcraft," *2018 IEEE/RSJ International Conference on Intelligent Robots and Systems (IROS)*, Inst. of Electrical and Electronics Engineers, New York, 2018, pp. 6214–6219.
https://doi.org/10.1109/TMECH.2019.2929589.

[23] Hayden, J. S., "The Effect of the Ground on Helicopter Hovering Power Required," *Proceedings AHS 32nd Annual Forum*, American Helicopter Soc., Washington, D.C., 1976.

[24] McCormick, B., *Aerodynamics, Aeronautics, and Flight Mechanics*, 2nd ed., Wiley, Hoboken, NJ, 1995, pp. 300–306.

[25] Landry, B., "Planning and Control for Quadrotor Flight Through Cluttered Environments," Ph.D. Thesis, Massachusetts Inst. of Technology, Cambridge, MA, 2015.

[26] Zhou, W., Ning, Z., Li, H., and Hu, H., "An Experimental Investigation on Rotor-to-Rotor Interactions of Small UAV Propellers," *35th AIAA Applied Aerodynamics Conference*, AIAA Paper 2017-3744, 2017.
https://doi.org/10.2514/6.2017-3744

C. Wen
Associate Editor